

Distributed Measurement of Rayleigh Backscattered Crosstalk for Bidirectional Multicore Fiber Transmissions Using Multi-Channel Optical Time Domain Reflectometry

Yuto Kobayashi⁽¹⁾, Tetsuya Hayashi⁽¹⁾, Takemi Hasegawa⁽¹⁾, Takahiro Sukanuma⁽¹⁾, Inoue Ayumi⁽¹⁾,
Takuji Nagashima⁽¹⁾, Hiroataka Sakuma⁽¹⁾, Takahiro Kikuchi⁽¹⁾, Osamu Shimakawa⁽¹⁾,
Hidehisa Tazawa⁽¹⁾, Masato Yoshida⁽²⁾, and Masataka Nakazawa⁽²⁾

⁽¹⁾Optical Communications Laboratory, Sumitomo Electric Industries, Yokohama, Japan,
kobayashi-yuto@sei.co.jp, t-hayashi@sei.co.jp, hase@sei.co.jp

⁽²⁾Research Institute of Electrical Communication, Tohoku University, Sendai, Japan

Abstract We experimentally demonstrate the in-span nonlinear accumulation of Rayleigh backscattered crosstalk in multicore fibers by novel distributed evaluation technique using multi-channel OTDR, which validates the previously-reported theoretical prediction. We also present the impact of fan-in/fan-out crosstalk on the backscattered crosstalk with experimentally-validated prediction formula. ©2022 The Authors

Introduction

Space division multiplexing (SDM) using multicore fibers (MCFs) is a promising candidate to overcome the fundamental limit of the transmission capacity of single-mode fibers. Crosstalk (XT) suppression is necessary for uncoupled MCF transmission without XT compensation. Bidirectional MCF transmissions where signals counter-propagate in nearest neighboring cores are attractive for XT suppression, and the earlier studies have revealed that one of the major XT sources in long-haul bidirectional MCF transmission systems is Rayleigh backscattered XT [1–3]. For unidirectional MCF transmissions, the linear accumulation of the direct XT (XT_{dir}) between copropagating modes over propagation distance has been well elucidated from theoretical and experimental studies [4–6]. For bidirectional MCF transmissions, the backscattered XT (XT_{BS}) has been reported to nonlinearly accumulates in each span, but grows linearly with the number of spans [1–3,7]. The nonlinear backscattered XT accumulation within each span has been theoretically predicted, but has not been experimentally confirmed in details, to the best of our knowledge.

In this paper, we present the distributed measurement method of Rayleigh backscattered XT using multi-channel OTDR, which validates nonlinear accumulation of the backscattered XT. We also show the effect of fan-in/fan-out (FIFO) XT on the backscattered XT.

Nonlinear accumulation of backscattered XT

Firstly, we discuss how XT_{BS} nonlinearly accumulate in each span. We assume optical power P_0 is launched to an end of Core 1 of an MCF having a length L . The transmitted power $P_1(L)$ at the other end of Core 1, and the

backscattered crosstalk power $P_{bs,n}(L)$ at the launching end of Core n can be expressed as [2]:

$$P_1(L) \approx P_0 \exp(-\alpha L), \quad (1)$$

$$P_{bs,n}(L) \approx P_0 \frac{S\alpha_R}{\alpha} h \left[\frac{1 - \exp(-2\alpha L)}{2\alpha} - L \exp(-2\alpha L) \right], \quad (2)$$

and XT_{BS} of the MCF can be expressed as [2,3,8]:

$$XT_{BS} = \frac{P_{bs,n}}{P_1} \approx \frac{S\alpha_R}{\alpha} hL \left[\frac{\sinh(\alpha L)}{\alpha L} - \exp(-\alpha L) \right], \quad (3)$$

where S is the proportion of the Rayleigh scattering component recaptured into a backward direction, α_R is the Rayleigh scattering loss coefficient, α is the propagation loss coefficient of optical power, h is the power coupling coefficient between nearest neighboring cores (between co-propagating modes), L is the span length. S can be approximated with effective area A_{eff} as [3,8]

$$S \approx 3\lambda^2 / (8\pi n^2 A_{eff}). \quad (4)$$

When $\alpha L \ll 1$, XT_{BS} can be approximated as

$$XT_{BS} \approx \frac{S\alpha_R}{\alpha} (hL)(\alpha L) \approx S\alpha_R hL^2, \quad (5)$$

using $\sinh(\alpha L)/(\alpha L) \approx 1$ and $\exp(-\alpha L) \approx 1 - \alpha L$.

When $\alpha L \gg 1$, XT_{BS} can be approximated as

$$XT_{BS} \approx \frac{S\alpha_R}{\alpha} hL \frac{\exp(\alpha L)}{2\alpha L} \approx \frac{S\alpha_R}{\alpha} \frac{h}{\alpha} \frac{\exp(\alpha L)}{2}, \quad (6)$$

using $\sinh(\alpha L) \approx \exp(\alpha L)/2$ and $\exp(-\alpha L) \approx 0$. So, in long-haul transmissions with $\alpha L \gg 1$ (span loss $\gg 10/\ln(10)$ dB ~ 4.34 dB), XT_{BS} grows exponentially. This is because P_1 decays exponentially, but $P_{bs,n}$ asymptotically approaches a constant value, as shown in Eqs. (1) and (2).

Evaluation method for backscattered XT from OTDR measurements

Here, we present the relationship between XT_{BS} and OTDR traces. Based on [6], when we launch

OTDR pulses with a width W and group velocity V_g only into Core 1 and when $hz \leq hL \ll 1$, the powers in Core 1 and Core n backscattered from a position z can be approximated as

$$P_{\text{OTDR},1}(z) \approx R_{\text{BS}} P_0 \exp(-2\alpha z), \quad (7)$$

$$P_{\text{OTDR},n}(z) \approx 2hz R_{\text{BS}} P_0 \exp(-2\alpha z), \quad (8)$$

with the Rayleigh backscatter coefficient:

$$R_{\text{BS}} = S\alpha_R \frac{V_g W}{2}. \quad (9)$$

By using the square root of Eq. (7):

$$\sqrt{P_{\text{OTDR},1}(z)} \approx \sqrt{R_{\text{BS}} P_0} \exp(-\alpha z), \quad (10)$$

P_1 can be expressed with $P_{\text{OTDR},1}$ as

$$\sqrt{P_{\text{OTDR},1}(0) P_{\text{OTDR},1}(z)} \approx R_{\text{BS}} P_1(z). \quad (11)$$

By integrating Eq. (8), we obtain

$$\int_0^L P_{\text{OTDR},n}(z) dz \approx \frac{V_g W}{2} P_{\text{bs},n}(L). \quad (12)$$

From Eqs. (3), (11), and (12), we can evaluate XT_{BS} by using

$$XT_{\text{BS}} \approx \frac{2R_{\text{BS}}}{V_g W} \frac{\int_0^L P_{\text{OTDR},n}(z) dz}{\sqrt{P_{\text{OTDR},1}(0) P_{\text{OTDR},1}(L)}}, \quad (13)$$

Experimental setup

We evaluated the backscattered XT using the multi-channel OTDR in [6]. Figure 1(a) shows the setup for measuring the XT of MCFs using the OTDR. The pulse signal from a laser diode (LD) is launched into Core 1 of the fiber under test via a FIFO device, and the backscattered power from Cores 1 and 2 are detected via the same FIFO. For comparison, we also measured the values of XT_{dir} and XT_{BS} with the direct power measurement using wavelength scanning method with continuous-wave (CW) tunable light source (TLS) with the setup shown in Fig. 1(b).

Table 1 summarizes the characteristics of the measurement samples. Both MCF-1 and MCF-2 have fusion splice points to realize longer spans for measurements. The FIFO for MCF-1 is an etched fiber bundle type FIFO [9] with a trench-assisted MCF pigtail, and the FIFO for MCF-2 is a fused taper type FIFO [10].

Results and discussion

Figure 2(a) shows the XT accumulation over propagation distance in MCF-1 (in a span). The

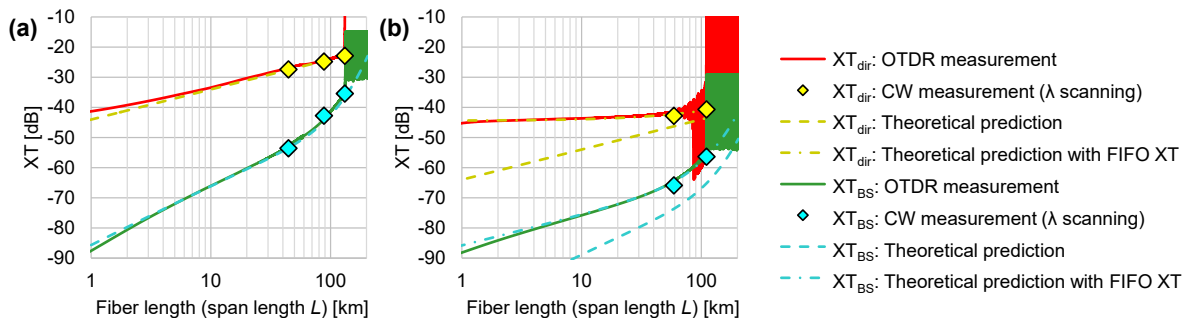


Fig. 2: XT accumulation over propagation distance in (a) MCF-1 and (b) MCF-2 (in a span).

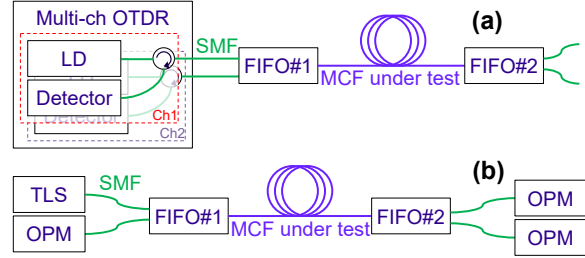


Fig. 1: Experimental setups for (a) distributed XT measurement using multi-channel OTDR and (b) direct power measurement using CW light source. LD: laser diode, TLS: tunable light source, OPM: optical power meter.

Tab. 1: The properties of the samples at $\lambda = 1.55 \mu\text{m}$

	MCF-1	MCF-2
Number of cores	4	2
α in dB/km	0.19	0.16
A_{eff} [μm^2]	74	109
R_{BS} in dB for 1-ns pulse W	-81	-84
Cutoff wavelength [μm]	<1.53	<1.53
Power coupling coeff. h in dB at 1 km [10 dB/decade]	-44.0 ^a	-63.6 ^b
Fiber length [km]	131	111
Fusion splice point [km]	44, 88	59
FIFO XT [dB]	<-80 ^a (#1+#2)	-44.3(#1) ^b -50.8(#2) ^b

a: Measured w/ transmitted power technique.

b: Measured w/ multi-channel OTDR technique.

OTDR pulse width was $10 \mu\text{s}$. The values of XT_{dir} from OTDR measurement was calculate by $(P_{\text{OTDR},n}/P_{\text{OTDR},1})/2$ as with the case of [6]. The values of XT_{BS} from OTDR measurement was calculated using Eq. (13). We corrected the zero point of the propagation distance as if the pulse center enters to the samples at the zero point. We also plot the XT_{dir} and XT_{BS} values measured using CW power measurement. The theoretical prediction of XT_{dir} is calculated from

$$XT_{\text{dir}} = hL, \quad (14)$$

where h was calculated from the CW power measurement result at $L = 131 \text{ km}$. The theoretical prediction of XT_{BS} is calculated using Eqs. (3) and (4), where we used the above h and the measurement values of α , α_R , A_{eff} (so, it is not the regression curve of the XT_{BS} measurement results).

The OTDR measurements agree well with the CW power measurements. Furthermore, OTDR-measured longitudinal profiles of the XT_{dir} and XT_{BS} are very well consistent with the theoretical predictions. Slight discrepancy at $L < 10$ km is caused by that Eqs. (7) and (8) ignore the longitudinal backscattered power change within the pulse width, but the discrepancy becomes negligible at $L > 10$ km, which can cover the span lengths of most of long-haul systems and where XT_{BS} becomes non-negligible for bidirectional MCF transmissions.

Figure 2(b) shows the XT accumulation over propagation distance in MCF-2 (in a span). The OTDR pulse width was 20 μ s for better sensitivity, because MCF-2 has lower XT even after long distance propagation. Most data were obtained in the same manner with the MCF-1 case. Since the XT of the FIFO (XT_{dir}^{FIFO}) is not negligible and almost the same with MCF-2 XT_{dir} after 100 km, h and FIFO XT were obtained from the OTDR-measured XT_{dir} (y -intercept can be regarded as XT_{dir}^{FIFO} as shown in Eq. (16) later).

Because the low-XT signal after 100 km was too weak to measure even with the 20- μ s pulse, we observed heavy noise on the OTDR-measured XT_{dir} after \sim 50-km propagation. However, the trend of the OTDR measurements agree well with the CW power measurements. Such a noise was not observed in OTDR-measured XT_{BS} because XT_{BS} is calculated from the integral of $P_{OTDR,n}$ and the weak power of $P_{OTDR,n}$ after long distance propagation does not have a significant impact on the integrated value.

The large difference between MCF-1 and MCF-2 measurements is XT_{dir}^{FIFO} . As XT_{dir}^{FIFO} is not negligible in the MCF-2 measurement. The OTDR-measured longitudinal profiles of the XT_{dir} and XT_{BS} do not agree with the theoretical predictions without XT_{dir}^{FIFO} .

Since XT_{dir} is linearly additive, the XT_{dir} of the measurement sample including MCF-2 and FIFOs for direct CW measurements is

$$XT_{dir}^{MCF+FIFOs} = XT_{dir}^{FIFO\#1} + hL + XT_{dir}^{FIFO\#2}. \quad (15)$$

For OTDR measurements, only the near-end FIFO (FIFO-N) has an impact on the backscattered powers. So, the values of XT_{dir} calculated by $(P_{OTDR,n}/P_{OTDR,1})/2$ should give

$$XT_{dir}^{MCF+FIFO-N} = XT_{dir}^{FIFO-N} + hL. \quad (16)$$

By fitting Eq. (16) to the OTDR traces measured from FIFO#1 end and FIFO#2 end, we evaluated the power coupling coefficient h of MCF-2 and FIFO XTs as summarized in Table 1. XT_{dir} measured by the CW method ($XT_{dir}^{MCF+FIFOs}$) and OTDR method ($XT_{dir}^{MCF+FIFO\#1}$) should have the difference of $XT_{dir}^{MCF+FIFO\#2}$, but the difference of $XT_{dir}^{MCF+FIFOs}$ and $XT_{dir}^{MCF+FIFO\#1}$ is only 0.5 dB in this

experiment and the results of OTDR and CW methods do not have a noticeable difference in Fig. 2(b).

When we consider the XT_{BS} with the effect of XT_{dir}^{FIFO} , we can ignore the backscattered XT or reflection XT in the FIFO, because the return loss of the FIFO is very high. Therefore, by considering that $XT_{dir}^{MCF+FIFO-N}$ is the co-propagating XT, we can derive XT_{BS} with the effect of XT_{dir}^{FIFO} as

$$XT_{BS}^{MCF+FIFO} \approx XT_{BS}^{MCF} + 2XT_{dir}^{FIFO-N} \frac{S\alpha_R}{\alpha} \sinh(\alpha L). \quad (17)$$

in the similar way of deriving Eq. (3). Note that $S\alpha_R$ can also be obtained using $S\alpha_R = 2R_{BS}/(V_g W)$ [Eq. (9)] with R_{BS} at W and V_g (or group index). Now, the OTDR-measured XT_{BS} also agree very well with the theoretical predictions with FIFO XT [Eq. (17)].

Figure 3 summarizes the per-span XT_{BS} increase due to FIFO XT ($XT_{BS}^{MCF+FIFO-N}/XT_{BS}^{MCF}$) as a function of $XT_{dir}^{FIFO-N}/XT_{dir}^{MCF}$ and αL in dB. For example, in the case of 15-dB span loss, the FIFO-induced XT_{BS} increase is almost negligible (<0.1 dB) when FIFO XT_{dir} is more than \sim 25-dB lower than the MCF span XT_{dir} . The effect of FIFO on XT_{BS} can be well estimated by using Eq. (17), if it is not negligible.

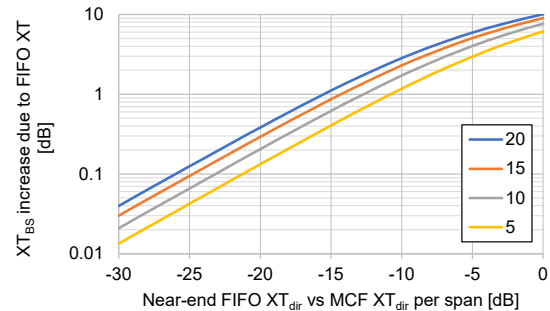


Fig. 3: XT_{BS} increase due to the near-end FIFO XT as a function of the ratio of FIFO XT_{dir} to MCF XT_{dir} per span and the span loss in dB (legend).

Conclusion

Newly developed OTDR measurement technique validated that the in-span XT_{BS} in MCFs can be well predicted by Eq. (3); therefore, bidirectional MCF transmissions with propagation direction interleaving between neighboring cores are very effective for XT suppression as presented in [1–3,7,8]. The suppression of FIFO XT is also important for designing XT_{BS} in bidirectional MCF transmission systems, and the effect of FIFO XT can be well estimated using Eq. (17).

Acknowledgements

This work was partially supported by the Ministry of Internal Affairs and Communications (MIC)/Research and Development of Innovative Optical Network Technology for a Novel Social Infrastructure (JPMI00316) (Technological Theme II: OCEANS), Japan.

References

- [1] T. Ito, E. L. T. de Gabory, M. Arikawa, Y. Hashimoto, and K. Fukuchi, "Reduction of Influence of Inter-core Cross-talk in MCF with Bidirectional Assignment between Neighboring Cores," in *Opt. Fiber Commun. Conf. (OFC)*, 2013, paper OTh3K.2, DOI: [10.1364/OFC.2013.OTh3K.2](https://doi.org/10.1364/OFC.2013.OTh3K.2).
- [2] A. Sano, H. Takara, T. Kobayashi, and Y. Miyamoto, "Crosstalk-Managed High Capacity Long Haul Multicore Fiber Transmission With Propagation-Direction Interleaving," *J. Lightwave Technol.*, vol. 32, no. 16, pp. 2771–2779, Aug. 2014, DOI: [10.1109/JLT.2014.2320826](https://doi.org/10.1109/JLT.2014.2320826).
- [3] T. Hayashi, T. Nagashima, A. Inoue, H. Sakuma, T. Saganuma, and T. Hasegawa, "Uncoupled Multi-core Fiber Design for Practical Bidirectional Optical Communications," in *Opt. Fiber Commun. Conf. (OFC)*, San Diego, 2022, paper M1E.1, DOI: [10.1364/OFC.2022.M1E.1](https://doi.org/10.1364/OFC.2022.M1E.1).
- [4] K. Takenaga, Y. Arakawa, S. Tanigawa, N. Guan, S. Matsuo, K. Saitoh, and M. Koshiha, "An Investigation on Crosstalk in Multi-Core Fibers by Introducing Random Fluctuation along Longitudinal Direction," *IEICE Trans. Commun.*, vol. E94-B, no. 2, pp. 409–416, 2011, DOI: [10.1587/transcom.E94.B.409](https://doi.org/10.1587/transcom.E94.B.409).
- [5] T. Hayashi, T. Taru, O. Shimakawa, T. Sasaki, and E. Sasaoka, "Design and fabrication of ultra-low crosstalk and low-loss multi-core fiber," *Opt. Express*, vol. 19, no. 17, pp. 16576–16592, Aug. 2011, DOI: [10.1364/OE.19.016576](https://doi.org/10.1364/OE.19.016576).
- [6] M. Nakazawa, M. Yoshida, and T. Hirooka, "Nondestructive measurement of mode couplings along a multi-core fiber using a synchronous multi-channel OTDR," *Opt. Express*, vol. 20, no. 11, pp. 12530–12540, May 2012, DOI: [10.1364/OE.20.012530](https://doi.org/10.1364/OE.20.012530).
- [7] K. Saitoh and S. Matsuo, "Multicore Fiber Technology," *J. Lightw. Technol.*, vol. 34, no. 1, pp. 55–66, Jan. 2016, DOI: [10.1109/JLT.2015.2466444](https://doi.org/10.1109/JLT.2015.2466444).
- [8] T. Hayashi, "Accuracy of Analytical Expressions for Rayleigh Backscattered Crosstalk in Bidirectional Multi-Core Fiber Transmissions," submitted for publication.
- [9] T. Kikuchi, O. Shimakawa, and H. Tazawa, "Low insertion loss and high return loss fiber bundle fan-in/fan-out for four-core multi-core fiber," in *OptoElectron. Commun. Conf./Photonics in Switching and Computing (OECC/PSC)*, to be presented, 2022.
- [10] V. I. Kopp, J. Park, J. Singer, D. Neugroschl, T. Saganuma, T. Hasegawa, T. Ohtsuka, and H. Tazawa, "Ultra-Low-Loss MCF Fanouts for Submarine SDM Applications," in *Opt. Fiber Commun. Conf. (OFC)*, San Diego, 2022, paper Th1E.2, DOI: [10.1364/OFC.2022.Th1E.2](https://doi.org/10.1364/OFC.2022.Th1E.2).